Ultrafast Imaging in Standard (Bi)CMOS Technology

Wilfried Uhring[1] and Martin Zlatanski[2]
[1]University of Strasbourg and CNRS
[2]ABB Switzerland Ltd.
[1]France
[2]Switzerland

1. Introduction

Around 1822, the French inventor Niépce made the first photographic image by the use of a *camera obscura*. He formed the image passing through the hole on a metal plate with a bitumen coating. After 8 hours of exposure, the bitumen on the illuminated sections of the plate was hardened. By washing the unhardened regions, a print of the observed scene appeared. After Niépce's death in 1833, Daguerre worked on the improvement of the chemical process involving interaction of the plate with light. In 1839 he announced the invention of a new process using silver on a copper plate. This invention reduced the exposure time to 30 minutes and denotes the birth of modern photography. During the following years, improvement on the photographic processes led to increased sensitivity and allowed shorter exposure times. In 1878, Muybridge gave an answer to a popular question at this time: whether all four hooves of a horse are off the ground at the same time during a gallop. By taking the first high-speed sequence of 12 pictures, each picture spaced about 400 ms from the neighbouring one with an exposure time of less than 500 µs. In 1882, George Eastman patented the roll film, which led to the acquisition of the first motion pictures. Four years later, a student of Daguerre, Le Prince, patented a *Method of, and apparatus for, producing animated pictures*. Through its *16 lens receiver*, as he called his camera, and by the use of an Eastman Kodak paper film, Le Prince filmed the first moving picture sequences known as the *Roundhay Garden Scene*, which was shot at 12 frames per second (fps) and lasted less than 2 seconds. Two years later, Edison presented the *Kinetoscope*, a motion picture device capable of acquiring sequences at up to 40 fps. It creates the illusion of movement by conveying a strip of perforated film filled with sequential images over a light source through a mechanical shutter. In 1904, the Austrian physicist Musger patented the *Kinematograph mit Optischem Ausgleich der Bildwanderung* which is capable of recording fast transients and projecting them in slow motion. In acquisition mode, the light is turned off and a rotating mirror, projecting them in slow motion. In acquisition mode, a rotating mirror mechanically coupled to the film shifting mechanism, reflects images onto the film. During the projection, the light is turned on and the same operation is carried out, but at a much slower rate. This high-speed photographing principle was used during the First World War by the German company Ernemann Werke AG to develop the *Zeitlupe*, a 500 fps camera used mainly for ballistic purposes. In 1926, Heape and Grylls constructed *Heape and*

Grylls Machine for High Speed Photography, in which the film shifting mechanism was replaced by a film lining the inside of a rotating drum, driven by an 8 horse power engine (Connel, 1926). The relaxed constraints on the film strength allowed to the 4 tons instrument to reach a frame rate of 5000 fps. In later realizations the drum was powered by an electric motor, leading to much more compact instruments (Lambert, 1937). Nowadays drum cameras are still in use and their fundamental principle is still the same. They employ a rotating mirror mechanically coupled to the drum and use the Miller's principle to perform the shuttering between frames. Miller's principle states that if an image is formed on the face of a mirror, then it will be almost static when relayed by lens to a film. The fastest drum cameras produce frame records at up to 200 000 fps which is limited by the mechanical constraints imposed by the need of a synchronous rotation of the mirror and the drum at very high speeds. Rotating mirror cameras have been developed toward the end of World War II to answer the need of photographing atomic explosions. The image formed by the objective lens is relayed back to a rotating mirror which sweeps the reflected image focused through an arc of relay lenses and shuttering stops on a static film (Fig. 1). The first camera of this type was built by Miller in 1939 and reached a speed of 500 000 fps. The concept was patented in 1946 (Miller, 1946) and in 1955, Berlin Brixner achieved a speed of 1 million fps using the same principle (Brixner, 1955). Cordin's Model 510 rotating mirror camera reaches 25 million fps, by driving the mirror up to 1.2 million rpm in a helium environment using a gas turbine (Cordin 2011). The speed of the drum and the rotating mirror cameras has not been improved for more than 40 years, the limits of this technology being set by the maximum rotation speed of the mirror and the materials (Frank & Bartolick, 2007).
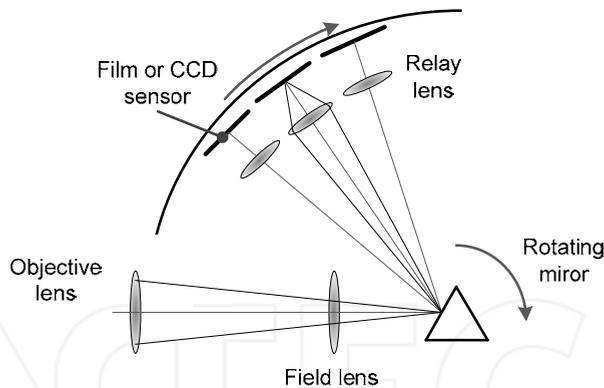
Fig. 1. Principle of the rotating mirror high speed video camera

Shortly after the first CMOS image sensors, the first Charge-Coupled Device (CCD) imagers appeared (Amelio et al., 1970). The CCD, initially developed for semiconductor bubble memory purposes, was invented in 1969 by Boyle and Smith at the Bell Laboratories. After promising initial results, this technology was rapidly adapted to be used for image sensor applications and little-by-little succeeded the photographic film (Smith, 2001). The first high-speed CCD cameras appeared during the 80's and were capable of acquiring up to 185 fps at a resolution of 512×512 pixels with a dynamic range of 8 bits. Their CMOS counterparts were able to go even further by integrating the signal conditioning electronics directly on-chip (Krymski et al., 1999; Kleinfelder et al. 2001). In both technologies, the shuttering is

operated electronically without the use of a mechanical part and can be potentially operated in few nanoseconds. Nevertheless, in both CCD and CMOS architectures, the maximum frame rate is limited by the time interval required for an image to be read out. Actual CMOS high-speed video cameras are capable of producing about 1 Mega pixel images at a rate of approximately 1000 fps or every other combination of image resolution and frame rate, which maintains the read-out rate to several GS/s. Indeed, by reducing the image size, the frame rate can be increased. A summary of the fastest high-speed video cameras in 2011 is given in Table 1. The maximum amount of data rate at the output (about 100 Gb/s for the fastest available camera) is generally limited by the bandwidth of the output bus. Parallelization of the channels seems to be a unpromising solution, since it leads to an excessive power consumption and unreasonable chip area (Meghelli, 2004; Swahn et al. 2009).

Manufacturer	Model	Resolution	Frame rate @ full resolution (total sampling rate)
Framos	MT9S402 (Sensor)	512×512	2500 ips (655MS/s)
Aptina (ex Micron)	MT9M413 (Sensor)	1280×1024 (10 bit)	500 ips (655 MS/s)
Micron	(Krymski et al. 2003)	2352×1728 (10 bits)	240 ips (975 MS/s)
Optronis	CR5000x2 (Camera)	512×512 (8 bits)	5000 ips (1.3GS/s)
Cypress	LUPA 3000 (Sensor)	1696×1710 8 bits	485 ips (1.4 GS/s)
Vision research	Phantom v640 (Camera)	2560×1600 (8 or 12 bits)	1500 ips (6.1 GS/s)
Vision research	Phantom v710 (Camera)	1280×800 (8 or 12 bits)	7530 ips (7.7 GS/s)
Photron	Fastcam SA5 (Camera)	1024×1000 (12 bits)	7500 ips (7.7 GS/s)
Photron	Fastcam SA2 (Camera)	2048×2048 (12 bits)	1000 ips (4.2 GS/s)
IDT	Y4-S3 (Caméra)	1016×1016 (10 bits)	9800 ips (10 GS/s)

Table 1. State-of-the-art of the fastest electronic high-speed video cameras in 2011

As seen from Table 1, today's high speed video cameras present a temporal resolution in the range of 1 ms in full resolution down to 1 µs in a reduced image size of about 1 thousand pixels. These performances are still far away from those of the rotating mirror cameras. To break the GS/s-order limit, a radically different approach than trying to operate the acquisition and the read-out progressively was required.

2. Ultrafast imaging concepts

2.1 *In situ* storage concept

The conventional high-speed video cameras face the input/output bus bandwidth constraint, which limits their data rate and temporal resolution to about 10 GS/s and 100 µs in full frame format, respectively. To overcome this bottleneck, the solution is simply not to extract the data from the sensor. Indeed, the fastest video sensors reported in the literature employ the *in-situ* concept, which consists in storing the acquired data on-chip rather than continuously extracting it and operate the readout afterwards. The use of this method in

CCD and CMOS optical sensors allowed to push the total sampling rate to about 1 TS/s, i.e. 100 times faster than the fastest high speed video cameras. The architecture of a sensor using the *in-situ* concept is shown in Fig. 2. Each pixel integrates a photodetector, generally a photodiode, and its own *in-situ* memory. Work on this concept started during the 90's and 1 million fps cameras have been reported (Elloumi et al. 1994; Lowrance & Kosonocky, 1997). These first sensors with *in-situ* frame memory, in which each pixel is composed by a photodetector and a linear CCD storage sensor were able to store 30 frames. In 1999, Professor Etoh proposed a sensor with 103-deep CCD storage (Etoh et al., 1999, 2005).
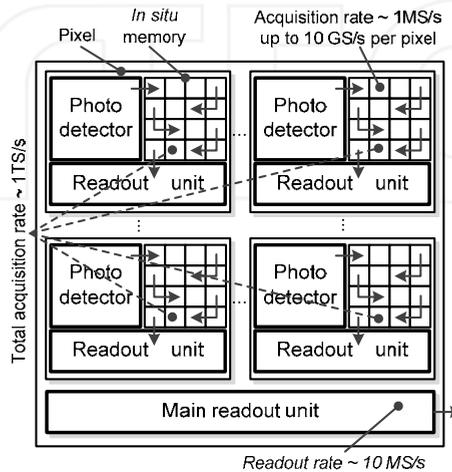

Fig. 2. Architecture of a high speed image sensor with the in-situ storage concept

A comparison between Cordin's Model 121 rotating mirror camera and Shimadzu's Model HPV-1 high-speed CCD imager with *in-situ* storage is made in (Franck and Bartolick, 2007). The test clearly shows the superiority of rotating mirror cameras in terms of spectral range, temporal and spatial resolutions. The authors conclude that at the moment a solid-state replacement for the rotating mirror cameras does not exist, but the *in-situ* based sensor architectures have the potential to reach higher performance through specifically optimized designs. Some studies forecast theoretical rates as high as 100 million fps for *in-situ* CCD detectors (Son et al. 2010), at the cost of reduced image quality.

The development of CMOS technologies allowed the integration of signal processing electronics and photodetecting site on the same substrate, which resulted in an enlargement of the spectrum of applications of solid-state imagers (Bigas et al., 2005). Since the bandwidth of a field-effect transistor in a submicron silicon technology easily exceeds the GHz, a number of these applications were naturally oriented towards high-speed imaging. In 2004, a 12×12 pixels demonstrator processed in standard 0.35 µm CMOS technology employing the *in-situ* storage concept achieved more than 10 million fps (Kleinfelder et al., 2004). The memory depth was of 64 and the pixel size of 200 µm $\times$ 200 µm. Recently, a 32×32 pixel prototype with an *in-situ* memory of 8 frames has been presented (Desouki et al. 2009). Processed in a 0.13 µm standard CMOS, it achieved a rate of 1.25 billion fps. The main drawback of this method is the limited memory depth to a maximum of about several

hundred frames. Indeed, the silicon area required increases with the number of stored frames and in 2D imaging, the in-pixel embedded memory decreases drastically the fill factor, e.g. less than 10% for only 8 frames in (Desouki et al., 2009). Nevertheless this is not a real issue, since in practice at these rates, generally only a few frames are analyzed. 3D technologies or die stacking may lead to fill factors as high as 100 %. However, ultrafast optical sensors employing the in-situ concept and featuring high fill factor can be processed in a standard (Bi)CMOS technology if streak-mode images are taken.

2.2 Streak-mode imaging concept

A feature proper to all the devices presented until now is that they produce 2-dimensional (x,y) images I_f at equally spaced in time intervals Δt. Consequently, I_f is a function of the two spatial dimensions x,y with a constant time $t_0 + n \cdot \Delta t$, where n is an integer:

$$I_f = f\left(x, y, t_0 + n \cdot \Delta t\right) \tag{1}$$

This is referred as framing mode photography. The advantage of a frame record is that information in two spatial dimensions is recorded, so the recorded image is an easily recognized version of the subject. However, if finer temporal information is required, another imaging method must be used. Speed and spatial information size of a camera being strongly related, a considerable gain in the frame rate can be achieved if the spatial information is reduced. If a single spatial dimension is selected, a picture containing the continuous temporal evolution of the spatial information is obtained. The recorded image I_s contains the spatial information x which crosses the slit, observed at different times t:

$$I_s = f(x,t) \tag{2}$$

This is denoted as streak-mode imaging. A streak record is made by placing a narrow mechanical slit between the event and the camera. Next, the temporal evolution of the one-dimensional spatial information crossing the slit is swept along a taping material. Thus, a continuous record containing position, time and intensity information is obtained. The recording rate, called sweep speed, translates the distance covered on the record surface for a unity of time and is measured in mm/µs or ps/pixel.
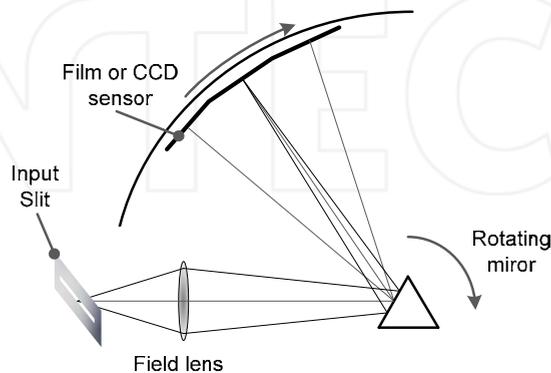

Fig. 3. Rotating mirror camera operating in streak-mode photography

To operate a rotating mirror camera in streak-mode, the relay lenses have to be removed and a slit positioned on the input optical path, (Fig. 3). With such a device, a maximal sweep speed of 490 ps/pixel has been reported (Cordin, 2011). Fig. 4 shows a frame (top) and a streak record (bottom) of a projectile fired through a near-side cut plastic chamber to impact an explosive sample. It clearly shows how a streak record provides continuous inter-frame temporal information of the slit image. The improvement in temporal resolution reaches about 2 orders of magnitude. Streak-mode imaging is ideal for studying events of uniform growth, e.g., an expanding sphere, where the rate of dimensional change is to be measured. To avoid misinterpretation and provide the maximum amount of information, often a combination of streak and framing records are carried out. Thus, framing and streak-mode cameras are not comparable, but rather complementary (Fuller, 2005).
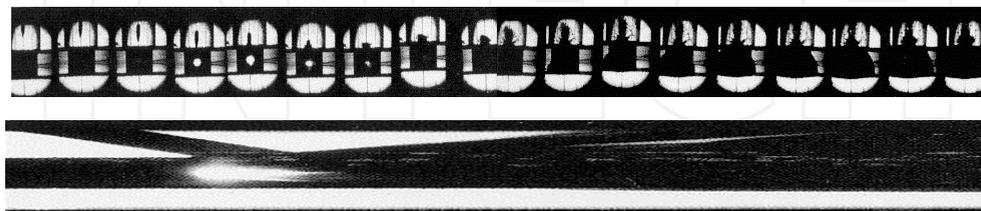

Fig. 4. Illustration of the streak imaging concept: frame record at 100 000 fps (top) and streak record at 0.53 mm/µs (bottom) of a ballistic event acquired by a Cordin Model 330 camera (Cordin, 2011)

The rotating mirror technology is limited by the centrifugal force applied to the mirror by the very high rotation speed. Even the use of light metals as beryllium does not prevent the mirror from explosion when the rotation speed exceeds 2 millions rpm (Igel & Kristiansen, 1997). To overcome this limitation a completely different technology based on a vacuum tube has to be used. The fastest device for direct light measurement available, known as the conventional streak camera allows picosecond-order temporal resolution to be reached. The operation principle of a conventional streak camera is depicted in Fig. 5. The very core of the streak camera is a modified first-generation sealed vacuum image converter tube, known as a streak tube, comprising four main sections: a photon-to-electron converter, an electron bunch focusing stage, an electrostatic sweep unit, and an electron-to-photon conversion stage. On some streak tubes, an internal Micro Channel Plate (MCP) is added in front of the phosphor screen for signal amplification. A mechanical slit is illuminated by the time varying luminous event to be measured and is focalized on the photocathode of the streak tube. The incident photons on the photocathode are converted to photoelectrons with a quantum efficiency depending on the type of the photocathode. A mesh is placed in the proximity of the photocathode and a high static voltage is applied between these two components in order to generate a high electrical field, which extracts the photoelectrons from the photocathode, makes their velocities uniform, and accelerates the pulse of photoelectrons along the tube. At this stage, the photogenerated electrons represent a direct image of the optical pulse, which reached the photocathode surface. When the photoelectrons approach the sweep electrodes, a very fast voltage ramp $V(t)$ of several hundred Volts per nanosecond is applied at a timing synchronized with the incident light. During the voltage sweep, the electrons which arrive at slightly different times, are deflected in different angles in the vertical direction. As far, first a photo-electrical conversion is

carried out by the photocathode, and then a translation from time to space is operated through the sweep electrodes. After being deflected, the electrons enter the MCP, where they are multiplied several thousands of times by bouncing on the internal channel walls acting as continuous dynodes and are extracted by the high electrical field applied on both sides of the MCP. At the end of the streak tube the photoelectrons impact against a screen which emits a number of photons proportional to the incident electron density. To prevent dispersion, an objective or a tapper made of a fine optical fiber grid is positioned in-between the phosphor screen and the read-out CCD or CMOS camera to guide the emitted photons.
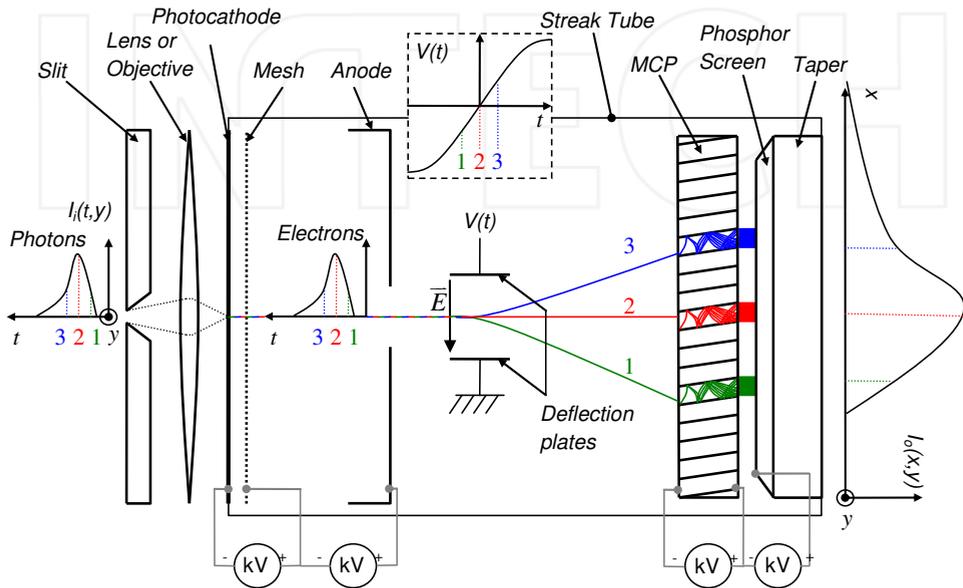

Fig. 5. Operation principle of a conventional streak camera

As the time-varying electric field caused by the voltage ramp between the electrodes is assumed to be spatially uniform, the spatial distribution of the light is directly obtained on the phosphorus screen without temporal modification. Finally, the temporal axis is found along the vertical direction of the screen, the position in the horizontal direction corresponds to the location of the incident light, and the brightness is proportional to the intensity of te respective optical pulses. The relationship between a given vertical position x and the time t depends on the slew rate S_R [V/s] of the sweep voltage $V(t)$ and the deflection sensitivity D_S [V/mm] of the streak tube is:

$$t = t_0 + \frac{D_s}{S_R} \cdot (x - x_0),$$ (3)

where x_0 is the position in mm of the slot image on the phosphorus screen when $V(t_0)$=0. As for the rotating mirror camera operating in streak-mode, the sweep speed of the camera is found as the ratio D_S/S_R, generally expressed in ps/mm.

Spectral range	[41 pm, 10 µm] depending on the photocathode type
Sensitivity	Single photon detection capability (with MCP or image intensifier)
Repetition rate	From single shot up to 250 MHz (synchroscan)
Spatial resolution	From 25 µm (ns resolution) to 100 µm (ps resolution)
Temporal resolution	From 200 fs (single shot) or 2 ps (synchroscan) to 300 µs
Sweep speed	From 10 ps/mm (fast sweep unit) up to 5 ms/mm (slow sweep unit)
Observation time	From 60 ps up to 175 ms (phosphorus screen size $\in$ [9–35 mm])

Table 2. Performance summary of a conventional streak camera

The conventional streak cameras are very versatile devices with high-end performances (Table 2). The wavelength detection spectrum ranges from the X ray (Scheidt & Naylor, 1999) up to the far infrared (Jiang et al. 1999). Their very high sensitivity permits the detection of a single photon event and the repetition rates extend from single shot operation up to several hundred of MHz. The typical spatial resolution of a conventional streak camera is between 25 µm and 100 µm. Specific tube designs using magnetic solenoid lens can reach a spatial resolution of 10 µm (Feng et al., 2007). Finally their temporal resolutions are very close to the physical theoretic limitation, about 100 fs (Zavoisky & Fanchenko, 1965) but with a poor signal to noise ratio whereas 1 ps can be reached with a high signal to noise ratio (Uhring et al., 2004a). Besides their extreme performances, conventional streak cameras and rotating mirror cameras have drawbacks: they are bulky, fragile, delicate to manufacture, and cost around 100 k€. Moreover there are many applications in which a temporal resolution of about 1 ns is sufficient. For these applications, solid-state technologies can offer interesting alternatives.

2.3 Streak camera alternatives

A high-speed video camera can be used as a streak-mode device by activating several rows on the sensor array and focusing the spatial information of interest on them. This technique is demonstrated in (Parker et al. 2010), where a temporal resolution of 1 µs and a sweep speed of 7.5 mm/µs have been reached, obviously limited by the output data rate.

In 1992, Lai from the Lawrence Livermore National Laboratory (USA) proposed a streak-mode camera in which the sweep is carried out by an externally triggerable galvanometer (Lai et al., 1992, 2003). The signal beam reaches the surface of the moving wedge-gap shaped deflector. It is subjected to multiple reflections between the surfaces of the stationary and deflecting mirror which results in an effective increase of the optical sweep speed. *N* reflections on the moving mirror result in an output beam angular speed equal to 2*N* times the rotating speed of the deflector. The deflected beam is focused and projected on a CCD sensor. At least 2 ms of trigger delay are required to allow the mirror to reach the targeted deflection speed. A temporal resolution of 30 ns has been reported.

Nowadays there isn't any solid-state streak-mode imaging device with performances situated in-between high-speed video cameras and conventional streak and rotating mirror cameras and in the same time there is a highly potential market for such a device. Indeed, many customers cannot afford the acquisition of a streak camera because of its price and, in the same time, they do not always need picosecond temporal resolution. In many streak-mode photography applications a temporal resolution in the order of several hundreds of picoseconds is often sufficient. The following section presents a solid-state alternative to the

conventional streak camera, which should give birth to new commercial and scientific activities, answers existing but unresponded demands and opens new fields of application. The prototypes are designed in a standard (Bi)CMOS technology which ensures quick prototyping and very low production cost estimated to about 10 % of the price of a traditional streak-mode imaging devices.

3. Integrated streak camera

Following the example of high-speed video cameras, the integration possibilities offered by CMOS technologies allow the use of the *in-situ* storage approach and its application to the first streak-mode CMOS imagers. In 1987, Professor Kleinfelder from the University of California proposed a 16 channel electrical transient waveform recording integrated circuit with 128 Sample and Hold (S/H) cells per channel operating in parallel at 100 MHz sampling frequency (Kleinfelder, 1987, 1990). In 2003, he demonstrated a 4 electrical channel 128-deep sampling circuit with up to 3 GHz operation using sub-micron silicon technology (Kleinfelder, 2003). One year later he presented a multi-channel sampling circuit in which the inputs of every channel are connected to an optical front-end (Kleinfelder et al. 2003, 2004). This was the first single-column streak-mode optical sensor. However, the very first integrated streak camera was developed in 2001 by the University of Strasbourg and was based on a pixel-array sensor architecture driven by an electronic temporal sweep unit (Casadei et al. 2003). In the following pages, both pixel array Integrated Streak Camera (MISC) and single-column Integrated Streak Camera (VISC) architectures are discussed.

3.1 Pixel array based integrated streak camera (MISC)

The optical setup required for a correct operation of a MISC is schematized in Fig. 6. The image of a light source illuminating a mechanical slit is uniformly spread along the temporal axis (the rows) of the 2D CMOS sensor through a cylindrical lens. Thus, each pixel of the same row is subjected to the same optical event. The distinctiveness of the integrated streak camera sensor compared to a conventional framing-mode sensors, consists in the way the pixels are operated. Indeed, a sweep unit is used to operate the time-to-space conversion carried out by the deflection plates in conventional streak cameras. The pixels of the sensor operate in photon flux integration mode. The circuit temporally sweeps the columns by shifting the beginning of their integrating phase every ΔT. Consequently, each pixel of a given row is subjected to the same illumination, which is measured at different moments.

The first generation MISC uses a 3T pixel that does not allow the integration to stop (Casadei et al. 2003). In practice, the latter ends with the read-out of the pixels. Consequently, attention must be paid to ensure that no light reaches the sensor's surface until the end of the read-out. The output ΔV_{ij} of the pixel p_{ij} at row i, column j is given by:

$$\Delta V_{ij} = \frac{1}{m} G_c \int_{j \cdot \Delta T}^{\infty} E_i(t) \cdot dt, \tag{4}$$

where G_c [V/n$_{ph}$] is the global conversion gain including the fill factor and the quantum efficiency, E_i [n$_{ph}$/s] is the optical power received by row i and m the number of pixels along the temporal axis, i.e., the number of columns. It is assumed that the time origin ($t=0$) corresponds to the first column ($j=0$). Processing the differential of the pixels along the

temporal axis, i.e., $S_{ij} = (\Delta V_{i(j+1)} - \Delta V_{ij})$ allows the reconstruction of the luminous event. Nevertheless, during this process, the high frequency noise is amplified and the signal obtained has a poor signal to noise ratio. Moreover, the dynamic range of the sensor is reduced since the first pixel integrates the entire signal and, at the same time, saturation must be avoided. The repetition rate of the acquisitions is limited by the read-out time of the array which is about 20 ms.
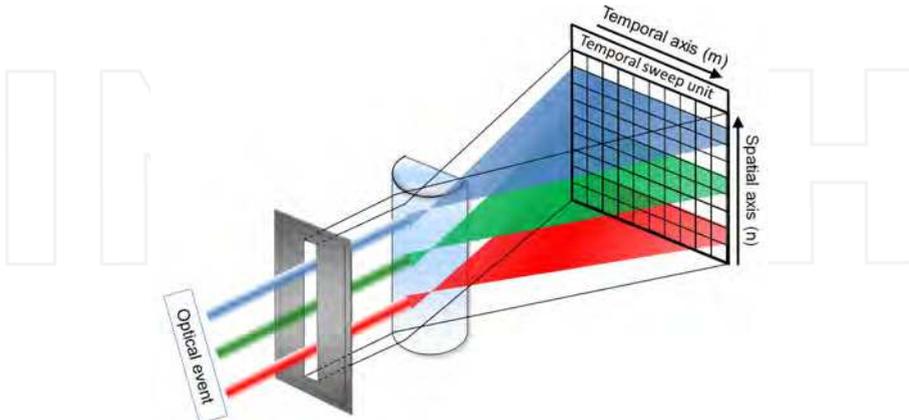

Fig. 6. Optical setup of a MISC

The second generation MISC employs a 6T pixel architecture in order to eliminate the faults of the first generation MISC by featuring a shutter capability. The detailed block diagram of a second generation pixel array-based sensor is shown in Fig. 7 (Morel et al. 2006). The circuit features an array of $n \times m$ active pixels, an m-stage temporal axis generator for the sweep unit, and two selection circuits and an output amplifier for serial data read-out. It temporally sweeps the columns by shifting the beginning and the end of their integrating phase, i.e., by delaying the arrival of the *RPD* and *SH* signals from one column to another. Thus, the integrating procedure starts with the turn off of transistor M_{RPD} and ends with the turn off of the transistor M_{SH} for all the pixels of column i and is delayed from column *i-1* by ΔT.

The 6T active pixel is also featuring an analog accumulation capability (Morel et al. 2006). Before acquisition, the potential on the cathode of the photodiode is initialized to V_{RPD} and the potential on the read-out node *RN* to *VRR*. After the integrating phase, i.e., the switching off of transistor $M_{SH,}$ the signal charges are trapped in node *IN*. Next, they are conveyed to the read-out node through M_{TX} acting as a transfer gate, allowing the on-chip accumulation of several repetitive low-light events through successive charge transfers from node *IN* to node *RN*. Anti-blooming is performed by keeping M_{RPD} in sub-threshold conduction after reset. In this circuit, the temporal sweep unit is composed of two identical delay lines with a single cell delay value of ΔT. The first delay line is used to control the reset transistor M_{RPD} whereas the second controls the shutter transistor M_{SH}. The beginning of the acquisition procedure, which consists of feeding the Trigger signal in the temporal sweep unit, is synchronized with the arrival of the optical event, through an external photodiode and a delay box. An externally tunable delay of T_{int} is added between the delay lines and allows

the tuning of the integrating time. For this architecture, the output ΔV_{ij} of the pixel p_{ij} is given by:

$$\Delta V_{ij} = \sum_{k=1}^{N}\left(\frac{1}{m}G_c\int_{j\cdot\Delta T}^{j\cdot\Delta T+T_{\text{int}}} E_{ki}(t)\cdot dt\right), \tag{5}$$

where N is the number of accumulations, G_c is the global conversion gain which includes the charge transfer efficiency from the photodiode to node IN and from node IN to node RN and E_{ki} is the k_{nth} optical signal received by row i. The second generation MISC features much higher dynamic range and tunable sweep speed from 140 ps up to 1 ns per pixel. The on-chip accumulation allows the observation of low intensity and repetitive optical signals, comparably to the synchroscan mode of a conventional streak camera. High repetition rates can be reached, since the duration of the charge transfer can be reduced down to 1 ns by appropriately adjusting the V_{RPD} and V_{RR} voltages (Uhring et al. 2011).
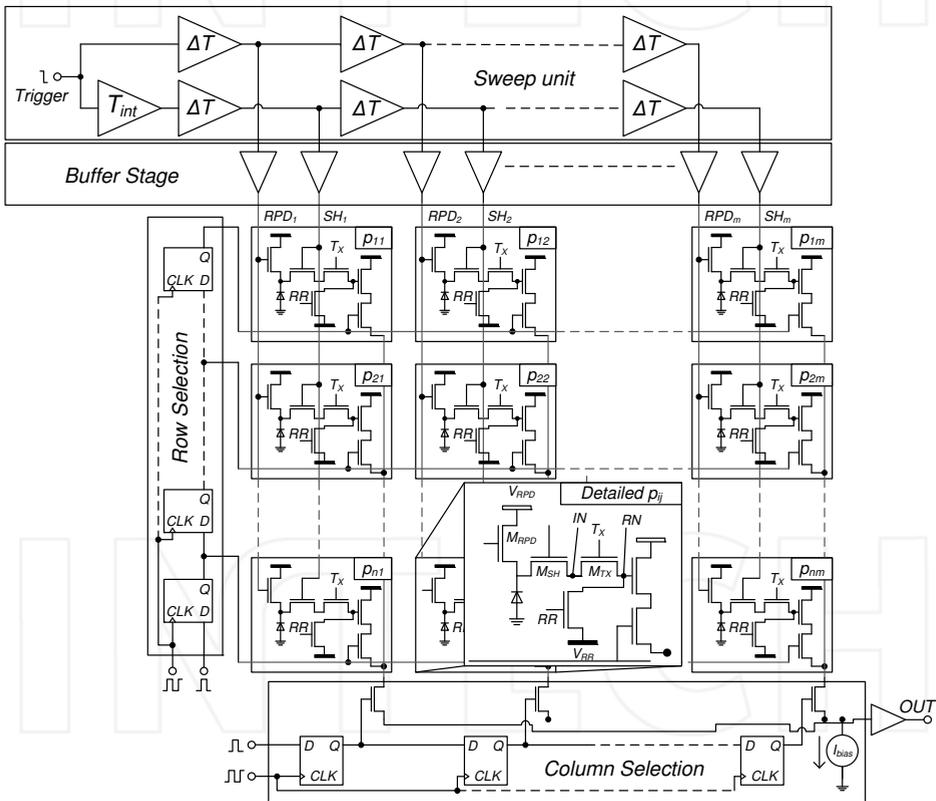

Fig. 7. Block diagram of the second generation MISC and detailed view of a pixel

Through the *in situ* concept and the parallelized operation, the MISC offers a very high speed as the only electronic limitation is the M_{RPD} and M_{SH} transistors bandwidth and turn off transient. The latest prototype with 93 rows channel exhibits a total sampling rate in

excess of 650 GS/s (Zlatanski et al. 2010a). The acquisition of a femtosecond laser pulse at 400 nm with an integration duration T_{int} of 400 ps indicates that the temporal resolution is 1.1 ns FWHM (Uhring et al., 2011). Preliminary results obtained with the picoseconds laser diode generator described in (Uhring et al. 2004b) show a temporal resolution very close to the nanosecond at 650 nm whereas the FWHM of the output pulse is increased to more than 3 ns at 808 nm. In 0.35 μm (Bi)CMOS technologies the bandwidth of a MOST switch can easily reach several GHz. The overall temporal response of a MISC in standard CMOS technology is then limited by the photodetector bandwidth. Unfortunately, the MISC suffers from a lack of sensitivity. Indeed, equations 4 and 5 clearly state that the output signal is divided by *m*, i.e. the memory depth (Zlatanski et al., 2010c). To avoid this, instead of spreading uniformly the light over the whole surface of the sensor, it should be focused to only one column. This is the basis of the vector based integrated streak cameras.

3.2 Vector based integrated streak camera (VISC)

The operation principle of a VISC is schematized in Fig. 8. In this case, the image of the slit is focused on the vector of photodetectors of the sensor through a spherical lens. Each one of the *n* photodetectors is connected to an amplifier and an *m*-deep sampling and storage unit. During illumination, the incident light is transformed to an electrical signal, which is amplified by the wideband front-end electronics. The outputs of the front-ends are sampled on the *in-situ* frame storage.
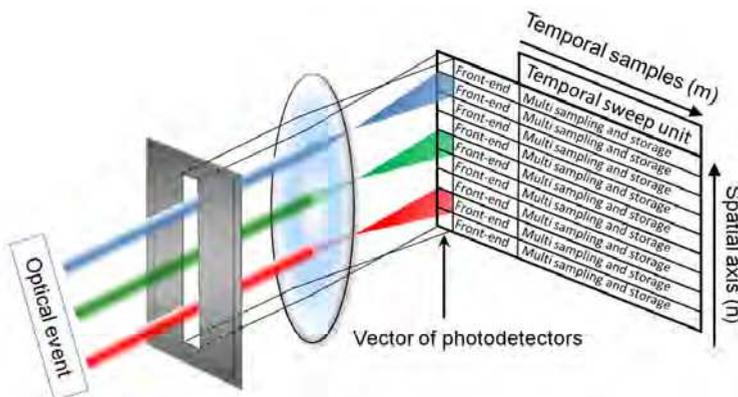

Fig. 8. Optical setup and architecture of a VISC

The different configurations of such a sensor are shown in Fig. 9. One approach is to use a transimpedance amplifier (TIA) coupled to a photodiode as a VISC front-end (Fig. 9 (a)). In this case, the photocurrent provided by the photodetector is converted to voltage with a given transimpedance gain, and is thus a direct image of the light event. At this level the circuit can be seen as a multichannel optical receiver circuit with an analog output. The sampling and storage unit is subjected to less design constraints as the signal to be sampled is in the voltage domain. The output ΔV of a pixel p_{ij} is simply given by:

$$\Delta V_{ij} = G_c \cdot E_i \left(j \cdot \Delta T \right), \tag{6}$$

where G_c is the global conversion gain of the sensor in [V·s/n$_{ph}$]. The frequency response of the photodiode is only slightly influenced, since the input impedance of a TIA is very low, typically ~100 Ω, and the bias voltage across the photodiode terminals is kept constant. However, a major drawback is the high power consumption as each front-end stage requires about 10 mW to reach a GHz-order bandwidth (Razavi, 2003).
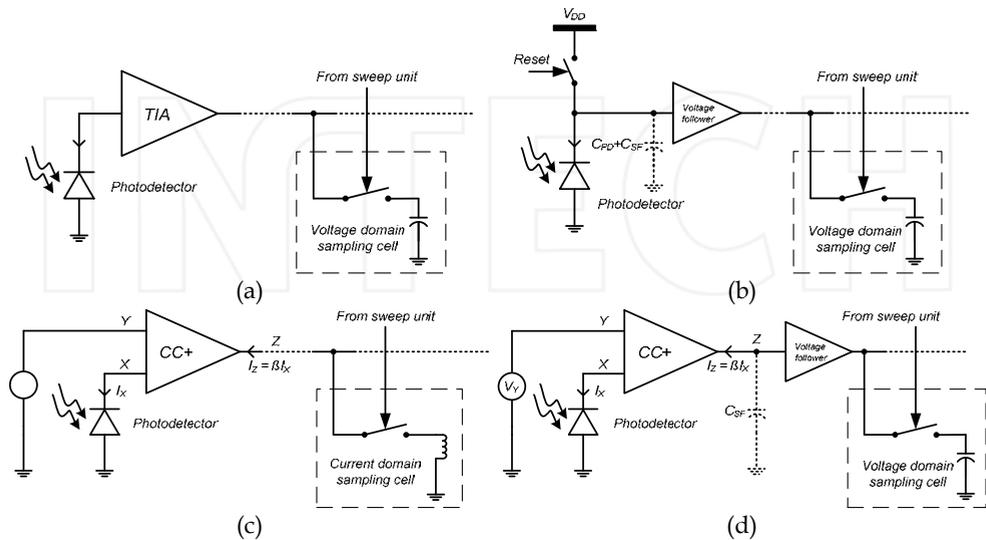

Fig. 9. Different front-end configurations: transimpedance approach (a), integrating approach (b), current to current approach (c) and hybrid integrating approach (d)

Another direct conversion could be obtained by using a Current Conveyor (CC) coupled to a line of m current-mode sampling cells (Toumazou et al. 1993; Mehr & Sculley, 1998; Rajaee & Bakthiar, 2005), as shown in Fig. 9 (c). The CC ensures that the voltage applied at Y is copied to X, keeping the photodetector under constant reverse bias. Next the current is conveyed to the output Z with a gain of ß, set by the design. Thus, the CC acts as current buffer between points X and Z. The value of pixel p_{ij} is given by equation (6), in which G_c, now given in [A·s/n$_{ph}$], includes the current conveyor and sampling cell gain.

The voltage follower front-end configuration (Fig. 9 (b)) has been used in the first VISC (Kleinfelder, 2004). The photocurrent is integrated on the photodetector and the voltage follower input capacitances and a standard voltage-domain sampling and storage block. The output voltage ΔV of pixel p_{ij} is given by:

$$\Delta V_{ij} = G_c \int_{j \cdot \Delta T}^{(j+\alpha) \cdot \Delta T} E_i(t) \cdot dt \qquad (7)$$

where G_c is the global conversion gain and $\alpha = T_{int}/\Delta T$ is the ratio of the integrating time to the sample period with $\alpha \in [0–1[$ in the structure proposed in (Kleinfelder, 2004). The hybrid integrating approach (Fig. 9 (d)) uses a CC to isolate the photodiode from the voltage follower. Thus, the photodiode biasing is maintained constant and the conversion

gain is increased as the integrating capacitance is reduced to the one at the input of the voltage follower.
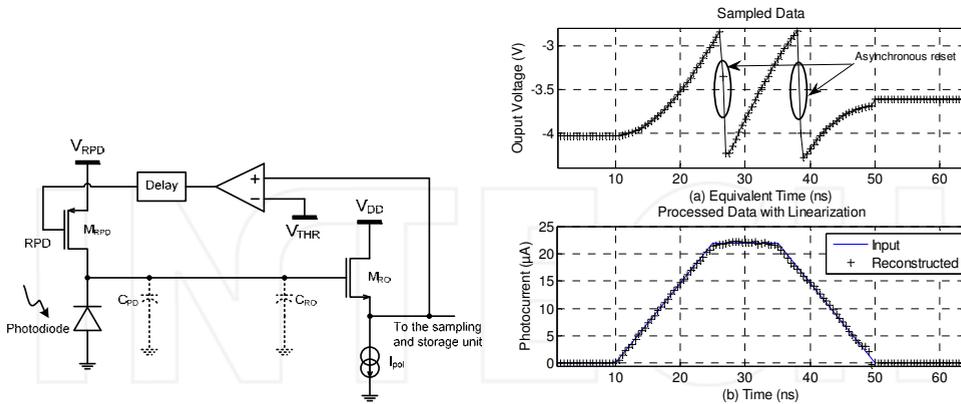

Fig. 10. Architecture of the asynchronous photodiode reset integrating VISC front-end (left) and a simulation result showing the output response to a pulse stimulus (right)

In the latter designs, the synchronous operation of the start and stop integrating phase severely limits the sampling rate to about 100 MS/s. In order to overcome this limitation, a novel asynchronous reset front-end architecture has been developed (Fig. 10-left). It includes a reset transistor M_{RPD}, a read-out transistor M_{RO}, and a feedback circuit which continuously senses the output of the front-end and resets the photodiode when a threshold voltage V_{THR} is attained indicating a soon run out of dynamic range. At circuit power-on, the *RPD* signal is externally triggered in order to provide a correct initial condition. For the fastest operation, the used comparator is an unmatched CMOS inverter. The simulated with Spectre® extracted view of this circuit showed a reset time as short as 600 ps. The photodiode reset phase being performed only when necessary together with its asynchronous with respect to the delay generator operation enable GS/s-order sampling performance associated to the high conversion gain of the integration. Data lost during the reset phase are detected and reconstructed (Zlatanski et al. 2010a).
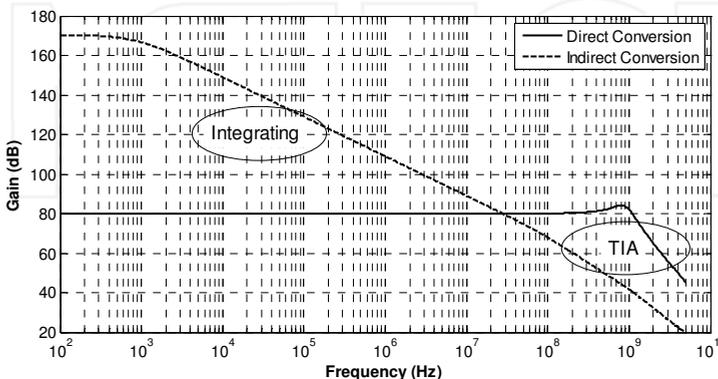

Fig. 11. Frequency responses of direct and indirect conversion architecture

The frequency response of the integrated streak camera depends on the front-end (Fig. 11). The response of the direct conversion front-end is given for a TIA with a gain of 80 dBΩ and a bandwidth of 1.3 GHz. The response of the indirect conversion front-end is given for a total capacitance of 100 fF including the photodiode and the front-end input parasitic capacitance. The cross point of these two responses is in the range of 10 MHz to 100 MHz depending on the integrating capacitance and the TIA. It is seen that the indirect conversion is appropriate for high gain measurements at low frequencies whereas the direct conversion seems to be the right choice when high bandwidth is required.

3.3 Temporal sweep unit

A common and important building block of the ISCs is the temporal sweep unit. The temporal sweep unit depicted in Fig. 12 allows the generation of sweep speeds in the range from 125 ps/pixel up to DC. It consists of a fast and a slow sweep unit. The Fast Sweep Unit (FSU) is useful for sub-nanosecond sampling period operation. It is composed of a Delay-Locked Loop (DLL) and two Voltage-Controlled Delay Lines (VCDLs). The observation time of the camera is set by the DLL reference clock period. The mirror VCDLs are driven by the same control voltages V_{hl} and V_{lh} as the master DLL allowing for asynchronous delay generation with respect to the reference clock. This makes it possible for the proposed generator to be launched from zero-tap position upon external triggering signal, ensuring the synchronization between the beginning of the acquisition procedure and the luminous phenomenon to be captured. The output taps of the VCDLs are delayed by an adjustable delay ΔT given by the ratio of the DLL Clock to the number of column m. The voltage controlled cell is a current starved double inverter with NMOS control transistors. It presents a large delay range and has been optimized for the shortest delay achievable in the CMOS technology employed (Mahapatra et al., 2002). The master DLL ensures the stability over temperature and the absolute precision of the delay. It is important that the VCDLs are
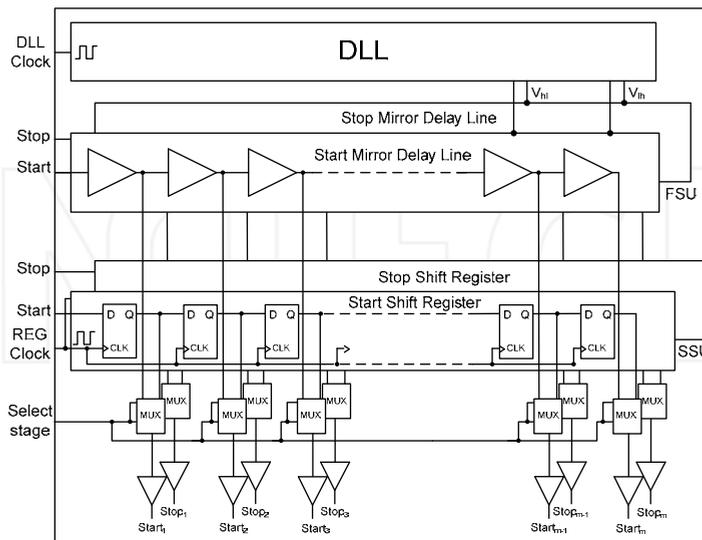

Fig. 12. Versatile sweep unit architecture including a Fast and a Slow Sweep Units

matched to ensure the same temporal shifting. For the MISC architecture, the *Start* and *Stop* signals, which control the M_{RPD} and M_{SH} transistors, respectively, are generated externally. Using two independent control signals allows the reduction the integration time down to 1 ns or less. The VISC architecture requires only one sampling signal, thus the mirror line generating the *Stop* signal is removed. Results from a similar FSU have been reported in (Zlatanski et al., 2011). Sweep speed of 125 ps/pixel up 1 ns/pixel with a drift of less than 0.05%/°C and temporal axis linearity better than 1% have been reported. The measured timing jitter in a completely asynchronous operation mode is less than 70 ps p-p@150ps/pixel and less than 700 ps p-p@770ps/pixel.

The Slow Sweep Unit (SSU) is useful for sweep speed of 1 ns/pixel up to DC. It uses a fast D flip-flop shift register. The sample period ΔT is equal to the period of the register clock *REG Clock*. The linearity of such a delay generator is very high as it is linked to the clock stability. Nevertheless, in an asynchronous operation, the timing jitter of the generated *start$_j$* and *stop$_j$* signals with respect to the trigger signal *Start* and *Stop* is equal to the sampling period peak-to-peak, i.e. ΔT p-p.

4. Direct optical conversion VISC

4.1 Front-end and sampling cell

A direct optical conversion VISC have been designed with the Austria Micro Systems 0.35μm BiCMOS process. One acquisition channel of the sensor is composed of a transimpedance amplifier as a front-end and a 128-deep memory (Fig. 13, left). The prototype features 64 channels. The temporal resolution of an integrated streak camera is determined by the overall bandwidth of the photodetector and the subsequent electronics. The target is to extend the bandwidth of the front-end beyond 1 GHz, which corresponds to a temporal resolution of less than 1 ns. The challenge consists in keeping the overall sensor bandwidth equal to that of the photodetector alone, while keeping a high gain. Moreover, the power consumption and silicon area should be kept low because of the multichannel architecture. The VISC makes use of a compact and fast voltage-domain sampling scheme shown in Fig. 13-left. An NMOS voltage sample and hold unit is appropriate for the operation as it offers a dynamic range of more than 2 volts and a bandwidth of more than 6 GHz.
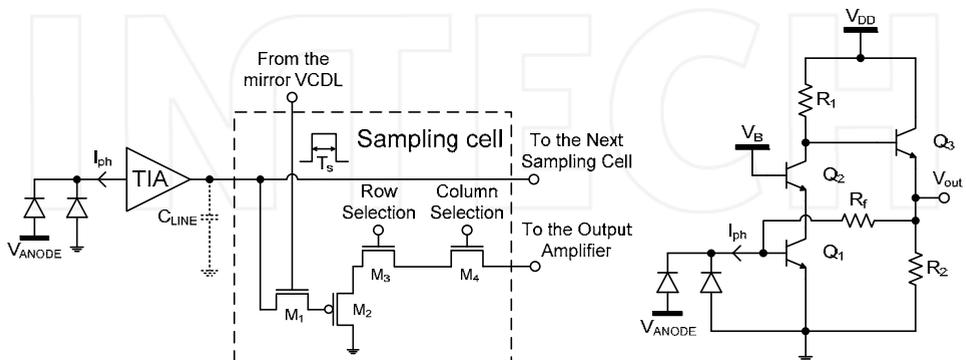

Fig. 13. A channel of the VISC with a double photodiode, a high speed TIA and the detail of a sampling cell with its read-out electronics (left). The transimpedance amplifier schematic (right).

The choice of the TIA topology is strongly restricted to low power and low area consumption architectures as some hundreds of channels are targeted in the final VISC. The designed shunt-shunt feedback common-emitter TIA, shown in Fig. 13-right, features a Gain-Bandwidth product of 17 THzΩ while consuming less than 7 mW. The simulated with extracted parasitics closed-loop gain and bandwidth are 80 dBΩ and 1.75 GHz, respectively. The circuit occupies only $26 \times 116\ \mu m^2$ and shows a good trade-off between gain, bandwidth, and power consumption (Table 3).

Reference	Technology	Gain	Bandwidth	GBZ	Power consumption	Notes
(Oh & Lee 2004)	0.35 μm CMOS	68 dBΩ	1.73 GHz	4.35 THzΩ	50 mW	CE with cascode, shunt peaking
(Huang, & Chen, 2009)	0.18 μm CMOS	66 dBΩ	7 GHz	14 THzΩ	-	Differential, inductive peaking
(Kao et al. 2010)	0.18 μm CMOS	74.6 dBΩ	2.9 GHz	15.6 THzΩ	31.7 mW	Differential, two stage, negative Miller capacitance
(Aflatouni et al. 2009)	0.13 μm CMOS	57 dBΩ	6 GHz	4.25 THzΩ	1.8 mW	RGC-input, series and shunt peaking
This work	0.35 μm BiCMOS	80 dBΩ	1.75 GHz	17.5 THzΩ	7 mW	SiGe Bipolar transistor

Table 3. Broadband transimpedance amplifiers in standard (Bi)CMOS 2011

4.2 Photodiode

The most versatile photodiode in bulk CMOS processes is the N_{WELL}–P_{SUB} photodiode since it features a wide and well-positioned depletion region, allowing the detection of long wavelengths with good responsivity. Because of the low overall speed of this diode, it is often used in a spatially modulated light detector (SMLD) configuration which consists in a finger topology of alternatively illuminated and shielded photodiodes (Genoe, 1998, Huang & Chen, 2009). However, the differential diode arrangement has several important drawbacks. The first is the large occupation area that arises from the number of alternating N_{WELL} fingers. Another drawback, directly originating from the finger topology, is the increased parasitic capacitance. To limit its impact on the electrical bandwidth of the subsequent electronics, the input impedance of the amplifier must be very low. The sensitivity is also severely decreased and more than a factor of 5 in output signal is lost at 800 nm, because of the shielded regions (Tavernier et al., 2006). Finally, a SMLD requires a differential processing to carry out the signal of the illuminated and the shielded detector. This configuration is thus not adapted for use within a VISC, where the spatial resolution must be kept around 20 μm and the number of channels must exceed 100.

It has been shown in (Radovanovic et al. 2005; Hermans & Steyaert 2006) that a P_{DIFF}–N_{WELL} photodiode with a screening N_{WELL}–P_{SUB} photodiode features the fastest overall bandwidth among all basic photodiode structures in bulk CMOS technologies, which can exceed 1 GHz at a wavelength of 850 nm. Unfortunately, the responsivity of the screened photodiodes is 10 times lower than that of P_{DIFF}–N_{WELL}–P_{SUB} double photodiodes at 850 nm and 6 times lower at 650 nm. The practical operation range of this topology is restricted to the short wavelengths, where the photogenerated carriers are efficiently collected by the surface

photodiode. Employing a screened P_{DIFF}–N_{WELL} photodiode would lead to an improvement of the temporal resolution, but at the cost of a severe loss in sensitivity.

Since the SMLD arrangement and the screened P_{DIFF}–N_{WELL} photodiode are not adapted for use in an integrated streak camera design, a single-ended photodiode coupled to an equalizer could be employed. However, the roll-off of the N_{WELL}–P_{SUB} photodiode at long wavelengths starts at about 1 MHz, which requires a 3rd order equalizer to achieve an effective compensation up to 1 GHz (Radovanovic et al. 2005). A single-stage, 3rd order equalizer requires not less than 2 transistors, 3 capacitors and 5 resistors. Thus, its implementation may become problematic with respect to the small implementation area available and the high power consumption constraint. Moreover, equalization should better be adaptive in order to cover multiple wavelengths and lower the impact of eventual component parameters spread. Adaptive equalization requires adjustable passive component values and thus additional control signals (Chen & Huang, 2007).

In an integrated streak camera, the raw data at the output of the sensor can be processed off-chip, allowing various post-processing such as filtering, FPN reduction through dark image subtraction, and recurrent light event accumulation. In the same vein, equalization can be carried out off-chip through software processing, provided the transfer function of the photodetector is known. If the roll-off in the frequency response can be compensated, it is better to use a photodiode with a higher responsivity in order to widen the spectral range and increase the signal to noise ratio. For this reason the photodiode with the widest spectral range and the highest responsivity in bulk CMOS technologies, i.e., the double P_{DIFF}–N_{WELL}–P_{SUB} photodiode has been chosen (Radovanovic et al., 2006). The equalization process in explained is Section 6.

5. Characterization of the temporal resolution of the VISC

The temporal resolution of the VISC has been measured by using a femtosecond laser source at 400 nm and 800 nm. The test bench, shown in Fig. 14, operates as follow: a femtosecond laser generates a stream of 100 fs FWHM pulses at 800 nm and 80 MHz. One of the pulses is selected and amplified by a oscillator/amplifier at a repetition rate of 5 kHz. This amplified pulse can then be doubled by an optional second harmonic generator (SHG) in order to generate a wavelength of 400 nm. This laser pulse is fed into an optical fiber which is focused on to the slit of the VISC. The measurement of the laser pulse at the output of the optical fiber with a synchroscan conventional streak camera shows that the pulse width is less than 7 ps FWHM, showing that it can be considered as a Dirac impulse by the system. A set of fixed attenuators have been placed in the optical path to avoid saturation of the sensor. A trigger signal generated by the amplifier ensures the synchronization of the streak camera with the laser pulse. A delay and pulse generator allows the precise adjustment of the trigger with respect to the laser pulse.

The response of the camera at a wavelength of 800 nm is shown in Fig. 15. The laser pulses followed by a secondary trace due to reflection in the optical fiber are clearly observed. As the laser pulse is very short, the obtained response represents the impulse response of the system, which in turn stands for the temporal resolution of the ISC. Thus, the temporal resolution is 710 ps FWHM at 800 nm and 490 ps FWHM at 400 nm. To compensate for the

poor performance of photodiodes in standard technologies, the frequency response of camera has been equalized.
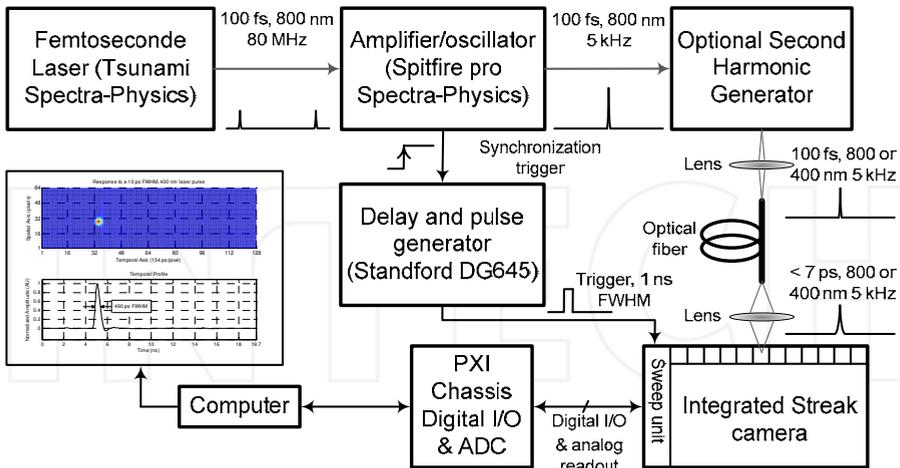

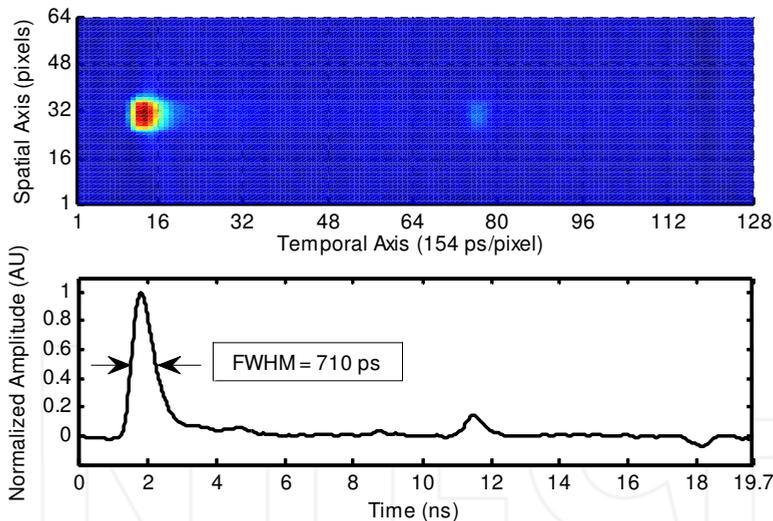Fig. 14. Experimental setup for impulse response measurement of the VISC

Fig. 15. Impulse response of the VISC at 800 nm

6. Improvement of the temporal resolution

The frequency response of the integrated photodiode has been corrected by using software equalization. The measured frequency response $H_M(z)$ of the TIA VISC, (Fig. 16) is obtained by computing the Fourier transform of the measured impulse response. It is seen that even if the -3 dB bandwidth of the photodiode is as low as 130 MHz at 800 nm, the high frequency

attenuation are limited to only 15 dB at 1 GHz. The weak attenuation at high frequency allows the compensation to be efficiently carried out. Assuming that no aliasing occurs in the baseband, if the inverse of the measured transfer function is employed as equalizing filter, a flat frequency response should be obtained. In practice, doing so, the high frequency noise is amplified and becomes dominant over frequencies in which meaningful information is contained. Finally, in the time domain, the event ends completely shaded by noise. To avoid this scenario, the frequency band in which the equalization is operated has to be limited. To do so, we synthesize a filter $H_I(z)$, which exhibits flat response up to a frequency f_{max} beyond which the SNR of the signal becomes unacceptably low, and next cuts off sharply any frequency situated above this bound. Indeed, this filter represents the desired global transfer function of the integrated streak camera. By computing the ratio between $H_I(z)$ and the measured transfer functions $H_M(z)$, we obtain the correcting function $H_C(z)$. Pushing the cut-off frequency of $H_I(z)$ close to f_{max} requires a high-order filter to efficiently attenuate noise. However, an abrupt cut-off approaches the shape of a brick-wall filter, which causes the time response to exhibit non-causal behavior, i.e. a *sinc* function impulse response. To prevent this scenario, the order of the filter must be lowered, which implies a lower cut-off frequency to efficiently attenuate noise. In the time domain, the compromise between filter order and cut-off frequency corresponds to a trade-off between pulse shape and signal to noise ratio. Thus, for given pulse shape and signal to noise ratio, a limit in the maximal achievable temporal resolution exists.
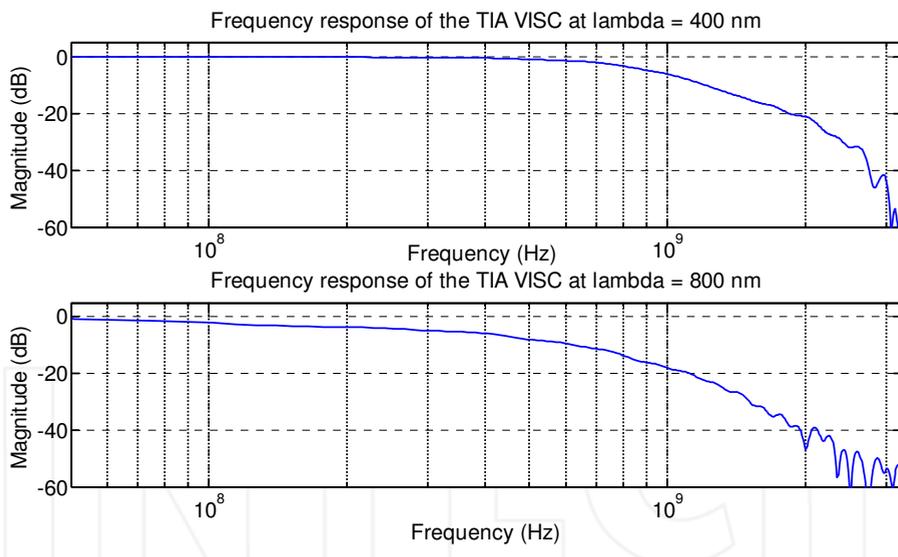

Fig. 16. Frequency response of the TIA VISC at 400 nm and 800 nm

Gaussian-type window has been chosen for the filter, since it matches best the expected and desired pulse shape at the output of a streak camera, excited by a delta function. Application of this global equalization at a wavelength of 800 nm using a 10th-order Gaussian filter $H_I(z)$ with a cut-off frequency of 1 GHz as desired frequency response yields the spectrum of the temporal response $H_E(z)$ shown on Fig. 17. Comparing the measured $H_M(z)$ and equalized $H_E(z)$ responses we notice a significant improvement up to ~2 GHz. Indeed, the low-

frequency roll-off is removed, resulting in the suppression of any slow variations in the observation window. The high frequencies have been amplified with a gain of about 15 dB, boosting the high-speed signal variations. Finally, the attenuation of $H_C(z)$ above 2.5 GHz improves the signal to noise ratio of the equalized signal.
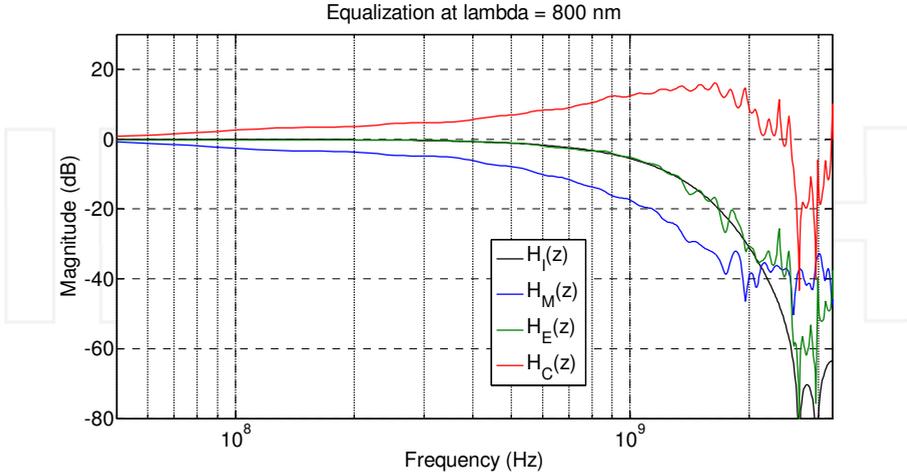

Fig. 17. Spectrum of the measured impulse response H_M (blue), targeted frequency response H_I (black) equalization filter H_C (red) and obtained frequency response after equalization H_E (green)
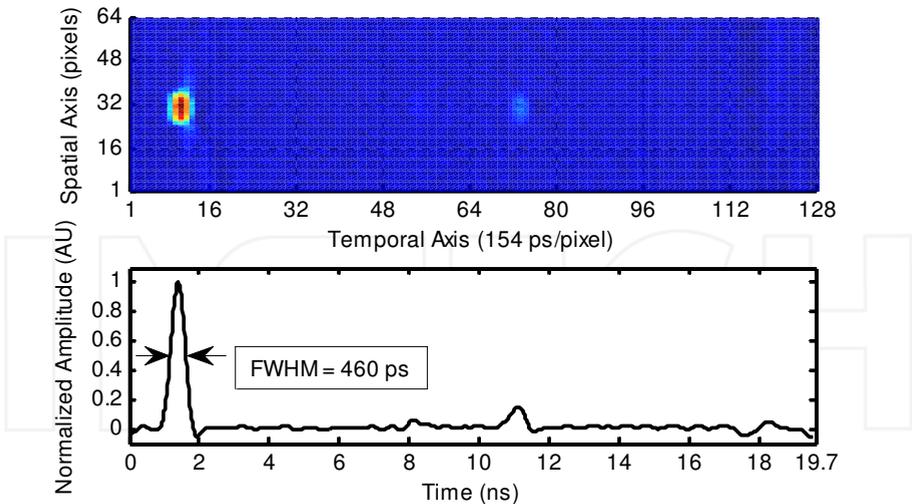

Fig. 18. Equalized impulse response of the TIA VISC at a wavelength of 800 nm

Result of the equalized impulse response of the TIA VISC at a wavelength of 800 nm is shown on Fig. 18. The FWHM is of 460 ps, which is more than 35 % lower than the measured value shown in Fig. 15. Interestingly, after equalization, the camera exhibits

similar temporal resolution and pulse shape at both wavelengths of interest. With such a temporal resolution, sub-nanosecond FWHM events can be detected and nanosecond-order phenomena measured with good accuracy. Equalization is a powerful technique, which allows the frequency response of an integrated streak camera to be made uniform over its entire spectral range. This is an important feature, since in streak-mode imaging the incident wavelength is often monochromatic or well known. For example, in one of the most common streak camera applications, the time-resolved spectroscopy, the streak image can be dynamically equalized, such as no distortion is introduced by the degraded behavior of the photodetectors with increasing wavelength.

Sensor	Sampling rate Temporal resolution	Number of channel	Memory depth per channel	Total sampling rate	Notes
UHFR – (Lowrance & Kosonocky, 1997)	1 MHz 1 µs	360 × 360	30	130 GS/s	First ultrafast CCD
ISIS-V4 (Etoh et al. 2006)	1 MHz 1 µs	420 × 720	144	300 GS/s	CCD technology. Colour version exists
3T MISC (UDS/CNRS) (Casadei et al. 2003)	1,25 GHz <6 ns	64	64	80 GS/s	First integrated streak camera
6T MISC$_a$ (UDS/CNRS) (Morel et al. 2006)	1,5 GHz <6 ns	64	64	96 GS/s	On chip analog accumulation feature
6T MISC$_c$ (UDS/CNRS) (Zlatanski et al. 2010a)	7 GHz <1.1 ns@400 nm	93	64	650 GS/s	Adjustable sweep speed
VISC$_b$ TIA (UDS/CNRS) (Zlatanski & Uhring 2011)	7 GHz 500 ps@400~800 nm	64	128	450 GS/s	TIA Gain 10000 V/A. First sub 500 ps VISC
VISC Source Follower (Zlatanski et al. 2010a)]	7 GHz < 1 ns	64	128	450 GS/s	Asynchronous reset
Kleinfelder SC (Kleinfelder et al, 2009)	100 MHz 10 ns	150	150	15 GS/s	Synchronous reset
J. Deen (Desouki et al., 2009)	1,25 GHz <1 ns	32 × 32	8	1,28 TS/s	0,130 µm, 1st video camera > 1 Gfps
Near future of integrated streak camera	10 GHz 100 ps	1024	1024	10 TS/s	Do not exist for the moment
Phantom v12.1 in streak-mode (Parker et al. 2010)	1 MHz 1 µs	128 × 8	2 s, i.e. 2 GS	1 GS/s	High speed video camera in streak-mode
Optronis SC10 streak camera	~5 THz 2 ps	~1024	~1024	~5 PS/s	Sweep speed 200 fs/pixel

Table 4. State of the art of ultrafast imaging solid-state sensors, the grey cells refer to other technologies than solid-state sensor with *in-situ* feature

7. Conclusion and perspectives

The concepts of ultrafast imaging and their application in ultrafast BiCMOS optical sensors have been presented. The TIA VISC prototype processed in standard BiCMOS technology reached an overall bandwidth of 1 GHz and a global sampling rate of more than 400 GS/s.

This work demonstrates that sub-nanosecond imaging with an equivalent frame rate of several billion fps is possible using standard (Bi)CMOS technologies. Table 4 summarizes the performances of the state of the art ultrahigh speed imaging solid-state sensors.

Phototransistors or avalanche photodiodes reported in standard technologies could be an interesting alternative to the standard photodiode structures as they can reach a photoelectron amplification factor of 100. The difference in sensitivity between the integrated and the conventional streak camera can thus be reduced down to one order of magnitude. Consequently, the sensitivity of the integrated streak camera has a high potential of evolution. In the near future, integrated streak cameras could be a competitive alternative to conventional streak-mode imaging instruments for applications in which a temporal resolution of about several hundreds of picoseconds is required.

8. References

Aflatouni F., & Hashemi H. (2009). A 1.8mW Wideband 57dBΩ Transimpedance Amplifier in 0.13μm *CMOS*, *IEEE Radio Frequency Integrated Circuits Symposium*, 2009, pp. 57

Amelio G. F., Tompsett M. F., & Smith G. E. (1970). Experimental Verification of the Charge-Coupled Semiconductor Device Concept, *The Bell System Technical Journal*, vol. 49, 1970, pp. 593–600

Bigas M., Cabruja E., Forest J. & Salvi J. (2006). Review of CMOS Image Sensors, *Microelectronics Journal*, vol. 37, 2006, pp. 433–451

Brixner B. (1955). One Million Frame per Second Camera, *Journal of the Optical Society of America*, vol. 45, no. 10, 1955, pp. 876–880

Casadei B., Le Normand J. – P, Hu Y., & Cunin B. (2003). Design and Characterization of a Fast CMOS Multiple Linear Array Imager for Nanosecond Light Pulse Detections, *IEEE Trans. on Instrumentation and Measurement.*, vol. 52, no. 6, 2003, pp. 1892–1897

Chen W. –Z, & Huang S. –Hao. (2007). A 2.5 Gbps CMOS Fully Integrated Optical Receiver with Lateral PIN Detector, *IEEE Custom Integrated Circuits Conference,* 2007

Connell H. W. (1926). The Heape and Grylls Machine for High-speed Photography, *Journal of Scientific Instruments*, Vol. 4, 1926, pp. 82–87

Cordin. (2011). *Rotating mirror camera specifications*, 10/05/2011, Available from: http://www.cordin.com/

Desouki M., Deen M. J., Fang Q., Liu L., Tse F., & Armstrong D. (2009). CMOS Image Sensors for High Speed Applications, *Sensors*, vol. 9, 2009, pp. 430–444

Elloumi M., Fauvet E., Goujou E., & Gorria P. (2004) The Study of a Photosite for Snapshot Video, *SPIE High Speed Imaging and Photonics*, vol. 2513, 2004, pp. 259–267

Etoh T. G., & Mutoh H. (2005). An Image Sensor of 1 Mfps with Photon Counting Sensitivity, *Proceeings of SPIE*, vol. 5580, 2005, pp. 301–307

Etoh T. G., Mutoh H., Takehara K., & Okinaka T. (1999). An Improved Design of an ISIS for a Video Camera of 1000000 fps, *Proc. of SPIE*, vol. 3642, 1999, pp. 127–132

Feng J. et al. (2007). An X-ray Streak Camera with High Spatio-temporal Resolution, *Applied Physics Letters*, vol. 91, 2007, no. 13

Frank A. M., & Bartolick J. M. (2007). Solid-state Replacement of Rotating Mirror Cameras, *Proc of SPIE.* vol. 6279, 2007, 62791U

Fuller P. (2005), Some Highlights in the History of High-Speed Photography and Photonics as Applied to Ballistics, *High-Pressure Shock Compression of Solids VIII Shock Wave and High Pressure Phenomena*, 2005, pp. 251-298

Genoe J., Coppe D., Stiens J.H., Vonekx R.A., Kuijk M. (2001).Calculation of the current response of the spatially modulated light CMOS detector, *IEEE Transactions on Electron Devices*, Vol. 48, 2001, pp. 1892

Hermans C., & Steyaert M. S. J. (2006). A High-speed 850-nm Optical Receiver Front-end in 0.18-μm CMOS, *IEEE Solid-State Circuits*, vol. 41, no. 7, 2006, pp. 1606–1614

Huang S. H., & Chen W. Z. (2009). A 10 Gb/s CMOS Single Chip Optical Receiver with 2-D Meshed Spatially-Modulated Light Detector, *IEEE Custom Integrated Circuit Conference,* 2009, pp. 129

Igel, E. A. & Kristiansen M. (1997). *Rotating mirror streak and framing cameras*, SPIE, ISBN 0-8194-2461-7

Jiang Z., Sun G. G., & Zhang X. C. (1999). Terahertz Pulse Measurement with an Optical Streak Camera, *Optics Letters*, vol. 24, no. 17, 1999, pp. 1245–1247

Kao T. S.-C., Musa F. A., Carusone A. C. (2010). A 5-Gbit/s CMOS Optical Receiver With Integrated Spatially Modulated Light Detector and Equalization, *IEEE Transactions on Circuits and Systems – I: Regular Papers*, vol. 57, no. 11, 2010, pp. 2844–2857

Kleinfelder S. (1987). Development of a Switched Capacitor based Multi-channel Transient Waveform Recording Integrated Circuit, *IEEE Transactions on Nuclear Science*, vol. 35, no. 1, 1987, pp. 151–154

Kleinfelder S. (1990). A 4096 Cell Switched Capacitor Analog Waveform Storage Integrated Circuit, *IEEE Transactions on Nuclear Science*, vol. 37, no. 3, 1990, pp. 1230–1236

Kleinfelder S. (2003). Gigahertz Waveform Sampling and Digitization Circuit Design and Implementation, *IEEE Trans. on Nuclear Science*, vol. 50, no. 4, 2003, pp. 955–962

Kleinfelder S., & Kwiatowski K. (2003). Multi-Million Frames/s Sensor Circuits for Pulsed-Source Imaging, *IEEE Nuclear Science Symposium*, vol. 3, 2003, pp. 1504–1508

Kleinfelder S., Chen Y., Kwiatkowski K., & Shah A. (2004). High-speed CMOS Image Sensor Circuits with In Situ Frame Storage, *IEEE Transactions on Nuclear Science,* vol. 51, no. 4, 2004, pp. 1648–1656

Kleinfelder S., Chen Y., Kwiatowski K., & A. Shah (2004). Four Million Frames/s CMOS Image Sensor Prototype with on focal Plane 64 Frame Storage. *Proc. of SPIE*, vol. 5210, 2004, pp. 76-83

Kleinfelder S., Sukhwan L., Xianqiao L., & El Gamal E. A. (2001). A 10 000 Frames/s CMOS Digital Pixel Sensor, *IEEE Journal of Solid-state Circuits*, vol. 36, 2001, pp. 2049–2059

Kleinfelder S., Wood Chiang S. –H., Huang W., Shah A., & Kwiatkowski K. (2009). High-Speed, High Dynamic-Range Optical Sensor Arrays, *IEEE Transactions on Nuclear Science*, vol. 56, no. 3, 2009, pp. 1069–1075

Krymski A. et al. (1999). A High-speed, 500 Frames/s, 1024 × 1024 CMOS Active Pixel Sensor, *Symposium on VLSI Circuits*,1999, pp. 137–138

Krymski A.I., Bock N.E., Nianrong T., Van Blerkom D., & Fossum E.R. (2003). A High-speed, 240-frames/s, 4.1-Mpixel CMOS Sensor, *IEEE Transactions on Electron Devices*, vol. 50, no. 1, 2003, pp. 130–135

Lai C. C. (1992). A New Tubeless Nanosecond Streak Camera Based on Optical Deflection and Direct CCD Imaging, *Proceedings of SPIE*, vol. 1801, 1992, pp. 454–468

Lai C. C., Goosman D. R., Wade J. T., & Avara R. (2003). Design and Field Test of a Galvanometer Deflected Streak Camera, *Proc. of SPIE*, vol. 4948, 2003, pp. 330–335

Lambert R. (1937). A Rotating Drum Camera for Photographing Transient Phenomena, *Review of Scientific Instruments*, vol. 8, 1937, pp. 13–15

Le Normand J-P, Zint V., & Uhring W. (2011). High Repetition Rate Integrated Streak Camera in Standard CMOS Technology, *Sensorcomm 2011*, 2011, pp. 322-327

Lowrance J. L., & Kosonocky W. F. (1997). Million Frame per Second CCD Camera System, *SPIE*, vol. 2869, 1997, pp. 405–408

Mahapatra N. R., Garimella S. V., Tareen A. (2000). An Empirical and Analysis Comparison of Delay Elements and a New Delay Element Design, *IEEE Computer Society Workshop on VLSI*, 2000, pp. 81–86

Meghelli M. (2004). A 132-Gb/s 4:1 Multiplexer in 0.13-Mm SiGe Bipolar Technology, *IEEE Journal of Solid-state Circuits*, vol. 39, no. 12, 2004, pp. 2403–2407

Mehr I. & Sculley T. L. (1998). Oversampling Current Sample/Hold Structures for Digital CMOS Process Implementation, *IEEE Trans. on Circuits and Systems–II: Analog and Digital Signal Processing*, vol. 45, no. 2, 1998, pp. 196–203

Miller C. D. (1946). U. S. Patent 2400887, 1946.

Morel F., Le Normand J.–P., Zint C.–V., Uhring W., Hu Y., & Mathiot D. (2006). A New Spatiotemporal CMOS Imager With Analog Accumulation for Nanosecond Low-Power Pulse Detections, *IEEE Sensors Journal*, vol. 6, 2006, pp. 11-20

Oh Y. – H., & Lee S. – G. (2004). An Inductance Enhancement Technique and its Application to a Shunt-peaked 2.5 Gb/s Transimpedance Amplifier Design, *IEEE Transactions on Circuits and Systems–II: Express Briefs*, vol. 51, no. 11, 2004, pp. 624–628

Parker G. R., Asay B. W., & Dickson P. M. (2010). A Technique to Capture and Compose Streak Images of Explosive Events with Unpredictable Timing, *Review of Scientific Instruments*, vol. 81, 2010, no. 016109

Radovanović S., Annema A. – J., & Nauta B. (2006). High-Speed Photodiodes in Standard CMOS Technology, *Springer*, 2006

Radovanovic S., Annema A.-J., & Nauta B. (2005). A 3-Gb/s Optical Detector in Standard CMOS for 850-nm Optical Communication, *IEEE Journal of Solid-State Circuits,* vol. *40,* no. 8, 2005, pp. 1706–1717

Rajaee O. & Bakhtiar M. S. (2005). A High Speed, High Resolution; Low Voltage Current Mode Sample and Hold, *IEEE Symp. Circuits and Syst.*, vol. 2, 2005, pp. 1417–1420

Razavi B. (2003). Design of Integrated Circuits for Optical Communications, *McGraw-Hill,* 2003.

Scheidt K.,& Naylor G.(1999). 500 fs Streak Camera for UV-hard X-rays in 1 kHz Accumulating Mode with Optical-jitter Free-synchronisation, *4th Workshop on Beam Diagnostics and Instrumentation for Particle Accelerators,* 1999, pp. 54–58

Smith G. E. (2001). The Invention of the CCD, *Nuclear Instruments and Methods in Physics Research, A,* Vol 471, 2001, pp. 1–5

Son D. V. et al. (2010). Toward 100 Mega-Frames per Second: Design of an Ultimate Ultra-High-Speed Image Sensor, *Sensors*, vol. 10, 2010, pp. 16–35

Swahn T., Baeyens Y., & Meghelli M. (2009). ICs for 100-Gb/s Serial Operation, *IEEE Microwave Magazine*, vol. 10, no. 2, 2009, pp. 58–67

Tavernier F., Hermans C., & Steyaert M. (2006). Optimised equaliser for differential CMOS photodiode, Electronic Letters, vol. 42, no. 17, 2006, pp. 1002–1003

Toumazou C., Lidgey F. J., & Haigh D. G. (1993). Analogue IC Design: The Current Mode Approach, *Institution of Engineering and Technology,* 1993

Uhring W. Zint C.V. Bartringer J. (2004b). A low-cost high-repetition-rate picosecond laser diode pulse generator, *Proc. of SPIE*, Vol 5452, 2004, pp. 583-590

Uhring W., Jung M., & Summ P. (2004a). Image Processing Provides Low-frequency Jitter Correction for Synchroscan Streak Camera Temporal Resolution Enhancement, *Proc. of SPIE*, vol. 5457, 2004, pp. 245–252

Zavoisky E. K., & Fanchenko S. D., Image Converter High-speed Photography with 10^{-9}–10^{-14} sec Time Resolution, *Applied Optics*, vol. 4, no. 9, 1965, pp. 1155-1167.

Zlatanski M. Uhring W. Zint C-V. Le Normand J-P., Mathiot D. (2010a). Architectures and Signal Reconstruction Methods for Nanosecond Resolution Integrated Streak Camera in Standard CMOS Technology, *DASIP*, 2010, pp. 1-8

Zlatanski M., & Uhring W. (2011). Streak-mode Optical Sensor in Standard BiCMOS Technology, *IEEE sensor conference,* 2011, In Press

Zlatanski M., Uhring W. Le Normand J-P. Zint C-V. Mathiot D. (2010b). 12 × 7.14 Gs/s rate Time-resolved BiCMOS Imager, *8th IEEE International NEWCAS*, 2010, pp. 97-100

Zlatanski M., Uhring W., Le Normand J.P., & Mathiot D. (2011). A Fully Characterizable Asynchronous Multiphase Delay Generator, *IEEE Transactions on Nuclear Science*, Vol. 58, 2011, pp. 418-425

Zlatanski M., Uhring W. Le Normand J-P. Zint C-V. Mathiot D. (2010c). Streak camera in standard (Bi)CMOS (bipolar complementary metal-oxide-semiconductor) technology, *Measurement science & technology*, Vol. 21, 2010, pp. 115203
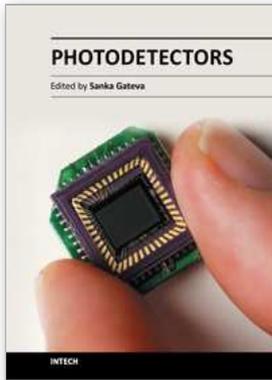
Photodetectors

Edited by Dr. Sanka Gateva

In this book some recent advances in development of photodetectors and photodetection systems for specific applications are included. In the first section of the book nine different types of photodetectors and their characteristics are presented. Next, some theoretical aspects and simulations are discussed. The last eight chapters are devoted to the development of photodetection systems for imaging, particle size analysis, transfers of time, measurement of vibrations, magnetic field, polarization of light, and particle energy. The book is addressed to students, engineers, and researchers working in the field of photonics and advanced technologies.

How to reference

In order to correctly reference this scholarly work, feel free to copy and paste the following:

Wilfried Uhring and Martin Zlatanski (2012). Ultrafast Imaging in Standard (Bi)CMOS Technology, Photodetectors, Dr. Sanka Gateva (Ed.), ISBN: 978-953-51-0358-5, InTech, Available from: http://www.intechopen.com/books/photodetectors/ultrafast-imaging-in-standard-bi-cmos-technology

INTECH
open science | open minds